
**CT Radiomics-Based Explainable Machine Learning Model for Accurate
Differentiation of Malignant and Benign Endometrial Tumors: A
Two-Center Study**

Tingrui Zhang^{1,2,†}, Honglin Wu^{3,†}, Zekun Jiang⁴, Yingying Wang⁵, Rui Ye⁶, Huiming Ni¹, Chang Liu⁴, Jin Cao⁴, Xuan Sun¹, Rong Shao⁷, Xiaorong Wei¹, Yingchun Sun^{1,*}

¹ Gynecology Department, Qingdao Hiser Hospital Affiliated of Qingdao University (Qingdao Traditional Chinese Medicine Hospital), Qingdao 266000, China

² Sichuan University - Pittsburgh Institute, Sichuan University, Chengdu 610000, China

³ Department of Obstetrics and Gynecology, Qingbaijiang Women's and Children's Hospital (Maternal and Child Health Hospital), West China Second University Hospital, Sichuan University, Chengdu 610300, China

⁴ College of Computer Science, Sichuan University, Chengdu, Sichuan 610000, China

⁵ Radiology Department, Qingdao Hiser Hospital Affiliated of Qingdao University (Qingdao Traditional Chinese Medicine Hospital), Qingdao 266000, China

⁶ Department of Traditional Chinese Medicine, Jiaozhou Traditional Chinese Medicine Hospital, Qingdao 266000, China

⁷ Adult Traditional Chinese Medicine Department, Qingdao Women and Children's Hospital, Qingdao 266000, China.

[†]These authors contributed equally to this work and share first authorship.

*Corresponding authors: Yingchun Sun. Gynecology Department, Qingdao Hiser Hospital Affiliated of Qingdao University (Qingdao Traditional Chinese Medicine Hospital), Qingdao 266000, China. Email: sunny8223@126.com.

Abstract

Objectives: Aimed to develop and validate a CT radiomics-based explainable machine learning model for diagnosing malignancy and benignity specifically in endometrial cancer (EC) patients.

Methods: A total of 83 EC patients from two centers, including 46 with malignant and 37 with benign conditions, were included, with data split into a training set (n=59) and a testing set (n=24). The regions of interest (ROIs) were manually segmented from pre-surgical CT scans, and 1132 radiomic features were extracted from the pre-surgical CT scans using Pyradiomics. Six explainable machine learning modeling algorithms were implemented respectively, for determining the optimal radiomics pipeline. The diagnostic performance of the radiomic model was evaluated by using sensitivity, specificity, accuracy, precision, F1 score, confusion matrices, and ROC curves. To enhance clinical understanding and usability, we separately implemented SHAP analysis and feature mapping visualization, and evaluated the calibration curve and decision curve.

Results: By comparing six modeling strategies, the Random Forest model emerged as the optimal choice for diagnosing EC, with a training AUC of 1.00 and a testing AUC of 0.96. SHAP identified the most important radiomic features, revealing that all selected features were significantly associated with EC ($P < 0.05$). Radiomics feature maps also provide a feasible assessment tool for clinical applications. DCA indicated a higher net benefit for our model compared to the "All" and "None" strategies, suggesting its clinical utility in identifying high-risk cases and reducing unnecessary

interventions.

Conclusion: CT radiomics-based explainable machine learning model achieved high diagnostic performance, which could be used as an intelligent auxiliary tool for the diagnosis of endometrial cancer.

Keywords: Endometrial Cancer; Radiomic; Personalized medicine; Machine Learning; CT

Highlight:

1. This is the first study to apply CT radiomics-based machine learning for diagnosing the malignancy and benignity of endometrial cancer (EC).
2. Among six modeling methods, the Random Forest model, using radiomic features from pre-surgical CT scans, demonstrated the highest diagnostic accuracy for EC.
3. CT scans are widely available, making the development of a CT radiomics-based intelligent diagnostic model highly valuable for accurately identifying tumor characteristics and guiding clinical decision-making in EC.

Introduction

Endometrial cancer (EC) is the second most common cancer among women [1]. Despite progress in cancer research, the incidence and mortality rates of EC continue to rise [2]. In high-income countries, EC is the most frequently diagnosed gynecologic cancer, and its incidence is steadily increasing worldwide. Since the mid-2000s, the annual incidence of uterine malignancies has risen by approximately 1% in women over 50 and by 2% in younger women since the mid-1990s. By the end of 2023, it is estimated that there will be 66,200 new cases and 13,030 related deaths in the United States alone [3].

Risk factors for EC include prolonged exposure to unopposed estrogen, often associated with conditions like polycystic ovary syndrome or infertility treated with tamoxifen, as well as obesity and hyperinsulinemia [4]. The most common symptom of EC is abnormal uterine bleeding, which should always be evaluated in postmenopausal women or women with other risk factors [5]. Preoperative imaging and histologic assessments are essential for tailoring surgical approaches to avoid unnecessary lymphadenectomy (LND) in low-risk patients [6]. Generally, an abdominopelvic computed tomography (CT) scan is performed to assess lymph node (LN) involvement or distant metastases, and positron emission tomography/CT scans are also viable options. Chest CT scans should be part of the initial assessment to rule out lung metastasis in high-risk cases. The role of serum tumor markers in EC is still uncertain [7].

As radiomic technology has advanced in recent years, increased attention is being

applied to its role in managing endometrial cancer [8-9]. Sophisticated quantitative, high-throughput radiomic features can be derived from tumor volumes in medical imaging, allowing for the identification of tumor characteristics that are imperceptible to the human eye. Radiomics provides a powerful method for capturing intratumoral heterogeneity by analyzing features from radiological images, and it has already contributed to the creation of diagnostic, predictive, and prognostic models, advancing the field of personalized medicine [10-13].

Machine learning (ML) has shown substantial benefits in diagnosing endometrial cancer (EC), particularly in identifying key features such as lymph node metastases and lymphovascular space invasion [14]. These advantages are most evident in studies that employ magnetic resonance imaging (MRI) due to its superior imaging details [15-16]. However, CT scans are more commonly used in routine clinical practice for initial diagnoses because of their faster acquisition times and broader availability. Therefore, it is crucial to develop ML models that can effectively analyze and extract features from CT scans. To date, CT-based radiomics combined with ML models have shown promising results in diagnosing lung cancer [17], skin cancer [18], prostate cancer [19], and colorectal cancer [20], but similar analyses for EC are limited to the pre-identification of MMR-D or TMB-H [21] and to recurrence prediction for prognosis [22].

Therefore, our study aims to develop and test an explainable machine learning model designed to diagnose EC using radiomics data extracted from pre-surgical CT scans. This model is intended to support early diagnosis of EC and facilitate informed

treatment decision-making.

Materials and Methods

This study was conducted in accordance with the tenets of the Declaration of Helsinki (as revised in 2013). The study protocol was approved by institutional review boards of Qingdao Hiser Hospital. All participants provided informed consent.

Patient population

A total of 83 patients who EC diagnose were included in this study (**Fig. 1**). The inclusion criteria were as follows: (1) patients with histologically confirmed uterine adenocarcinoma, (2) patients without distant metastasis, (3) patients who were not excluded due to pregnancy. The exclusion criteria were as follows: (1) patients lacking basic clinical information, such as age and sex, (2) those with unclear clinical staging, and (3) those with poor CT image quality. We divided the patients into a training set and an independent testing set based on the hospital where they received treatment. The training set consisted of 59 patients from Qingdao Hiser Hospital treated between January 2018 and March 2020, and the testing set included 24 patients from Qingdao Women and Children Hospital treated between November 2018 and March 2020. Clinical characteristics were acquired from all patients, see

Table 1

Pathological Diagnosis

Pathological diagnosis remains the gold standard for confirming endometrial cancer [23]. This involves histopathological analysis of tissue samples obtained through

endometrial biopsy methods, such as diagnostic curettage and hysteroscopy. Diagnostic curettage allows for comprehensive tissue sampling from both the endocervix and endometrial cavity, which aids in assessing the lesion's extent and nature. Hysteroscopy further enhances diagnostic accuracy by providing direct visualization, targeted biopsy, and excision of localized lesions. Histopathological examination of these samples offers critical insights into the characteristics and spread of the disease, which supports the development of personalized treatment plans for endometrial cancer.

CT image acquisition

Spiral CT scans for endometrial cancer were performed on all patients (using Philips Brilliance iCT and Siemens Somatom Definition AS). The scanning parameters were as follows: tube voltage at 120 kV, automatic tube current, pitch 1.0~1.5, matrix 512×512 , and field of view (FOV) $350 \text{ mm} \times 350 \text{ mm}$. After initial data collection, all patients underwent a no-interval reconstruction of $0.5 \sim 3.0 \text{ mm}$. A high-resolution algorithm was applied to enhance image quality. The scans were conducted with the patient in a supine position, arms placed on either side of the head, and breath-hold was employed during scanning. The scanning range covered the area from above the uterine fundus to below the pelvic cavity. All CT images were retrieved from the Picture Archiving and Communication System (PACS) for further feature extraction and analysis.

Tumor segmentation

Tumor segmentation was manually conducted across the entire tumor volume using

ITK-SNAP software (version 3.8.0; www.itksnap.org). Region-of-interest (ROI) positioning was established by two board-certified gynecologic radiologists with 11 and 13 years of experience in endometrial cancer imaging, respectively. Both radiologists were blinded to clinical and histological findings to reduce potential bias. To evaluate the impact of inter-observer variability on ROI delineation, which could affect radiomic feature extraction, each radiologist independently reviewed all CT images. Any discrepancies were resolved by consensus.

Radiomics feature extraction, selection, and analysis

In the study, Pyradiomics (version 3.0.1) was used to transform CT images to extract radiomic feature successively. The extracted features included: 14 shape features, 18 first-order statistical features, 22 gray level co-occurrence matrix (GLCM) features, 16 gray level run length matrix (GLRLM) features, 32 gray level size zone (GLSZM) features, 14 gray level dependence matrix (GLDM) features, 5 neighboring gray-tone difference matrix (NGTDM) features, 364 wavelet transform features, 91 square transform features, 91 square root transform features, 91 logarithmic transform features, 273 log-sigma features and 91 exponential transform features. A total of radiomic features 1122 were extracted from each ROI.

The predictive performance of the features was evaluated using ridge regression-based recursive feature elimination (RFE), through which valuable features were selected for modeling. RFE identifies the best features by repeatedly building models and evaluating feature coefficients [24]. To ensure stable estimates, the 20 most representative features were selected from the original 1122 high-throughput

radiomic features for modeling.

The relationships among these selected features were first analyzed, followed by a clinical correlation analysis to assess their biological significance. Then, the Shapley Additive Explanations (SHAP) analysis further evaluated the feature importance ranking to enhance model interpretability. Meanwhile, the radiomics feature maps were calculated to further enhance the understanding of feature visualization [25, 26].

Model construction and validation

The prediction models were built using machine learning models including random forest, decision tree, logistic regression, Gaussian process, support vector machine, and TabPFNv2 [27]. Accuracy, precision, sensitivity, and specificity metrics were used to evaluate the performance of each model. Finally, after comparing all these models, the final Radiomic score was calculated in the training set and tested in an external testing set. Meanwhile, the receiver operating characteristic (ROC) curve, confusion matrix, calibration curve, and decision curve were all calculated and evaluated.

Statistical analysis

All statistical analyses and machine learning algorithms were performed using Python (version 3.10). The evaluation of the model was primarily conducted using area under the ROC curve (AUC). These metrics effectively help us analyze the trade-offs between true positive rates and false positive rates at various thresholds, thus assessing the model's classification effectiveness [28, 29]. We also applied the

DeLong test to compare the efficacy differences between models, determining which model exhibited superior statistical performance. All tests had to achieve statistical significance at a P-value less than 0.05 to ensure the reliability and validity of the results. Through these rigorous statistical methods, we ensured that our model is not only theoretically sound but also robust in practical application, providing strong predictive performance.

Result

Clinical characteristics

There were 33 malignant and 26 benign EC cases in the training set, and 13 malignant and 11 benign EC cases in the testing set. We further divided the data into an experimental group (59 cases) and a control group (24 cases) based on the malignancy and benignity of EC for subsequent radiomics feature distribution analysis. **Table 1** lists all the obtained clinical characteristics, with no statistically significant differences between the two groups ($P = 0.218-1$).

Radiomics features discovery

Fig. 2 presents the SHAP analysis and importance ranking of the top 20 radiomics features. Among them, 60% belong to texture features, while 40% are first-order statistical features. Additionally, 90% of these features originate from transformed images, indicating that image transformations such as wavelet and LoG filtering can enhance the expression of texture features, which is consistent with previous studies [26].

Table 2 presents a comparison of the top 20 radiomic features between experimental and control groups, highlighting significant differences in their means and variability. Specifically, features such as log-sigma-5-0-mm-3D_firstorder_90Percentile and log-sigma-1-0-mm-3D_glcM_MaximumProbability show substantial differences between groups, with the experimental mean significantly higher or lower than the control mean across all features, as indicated by the p-values (all $p < 0.001$). For instance, the feature log-sigma-5-0-mm-3D_firstorder_90Percentile had a mean of 0.90 ± 2.77 in the experimental group compared to -0.97 ± 0.72 in the control group, reflecting a pronounced disparity in their distributions. These statistically significant differences suggest that the radiomic features can potentially distinguish between conditions applied in experimental versus control settings, providing a quantitative basis for further model development in predictive machine learning applications within medical imaging.

Development of machine learning models

The predictive performance comparison of all machine learning models is detailed in **Table 3**, demonstrating that all radiomic models were capable of diagnosing EC with AUCs exceeding 0.88. However, the Random Forest model was particularly distinguished, achieving an AUC of 1.00 in training set and 0.96 in testing set, which was superior to all other models.

Overall performance of the final radiomics model

The performance metrics and evaluation results of the final radiomics model are

shown in **Table 3** and **Fig. 3**. In the training set, the Random Forest model achieved a perfect AUC of 1.00, along with 95.83% specificity and 100% sensitivity, underscoring its excellent diagnostic accuracy. Similarly, in the testing set, this model maintained a high AUC of 0.96, with a specificity of 92.31% and sensitivity of 100%, thereby confirming the effectiveness of our final radiomic signature. Furthermore, the confusion matrices also reveal the high precision of the model, solidifying its role as the most reliable model for EC diagnosis.

To further evaluate the clinical applicability of our model, we conducted calibration curve analysis based on Isotonic Regression [24] (**Fig. 4A, B**) and decision curve analysis (**Fig. 4C, D**). The calibration curve further assessed the model's true prediction bias, while the decision curve demonstrated that our model consistently achieved a higher net benefit across different risk thresholds compared to the "treat all" or "treat none" strategies. These clinical analyses further highlight the potential clinical value of the radiomics model, providing important decision support for EC diagnosis.

Radiomics feature maps

The feature maps in **Fig. 5** visually demonstrate the distinct radiomics characteristics between malignant and benign tumors. The malignant tumor (top row) displays greater heterogeneity across multiple feature domains, with more complex internal patterns and irregular intensity distributions. In contrast, the benign tumor (bottom row) exhibits more homogeneous patterns with uniform intensity and smoother transitions. This visualization approach provides an intuitive representation of the

complex mathematical features that drive our classification model.

Discussion

This study developed and validated an explainable machine learning model for the precise identification of malignant EC, filling the research gap in CT radiomics for EC diagnosis and exploring its potential value in clinical decision support.

To evaluate the CT radiomics models' performance, we trained and compared several models, including Logistic Regression, K-Nearest Neighbors, Support Vector Classifier, XGBoost, Random Forest, and TabPFNv2. Although TabPFNv2 was the novel tabular foundation model with publishing in Nature and received widespread attention [27], it did not perform best in our experiments. Among these, Random Forest showed the highest diagnostic accuracy. This effectiveness can be attributed to the ensemble nature of Random Forest, which minimizes overfitting risks by constructing each decision tree with different subsets of data and features. Consequently, Random Forest prevents the model from becoming overly specific to the training data while preserving accuracy. Moreover, Random Forest's capacity to handle a large number of features makes it well-suited for capturing the complexity and diversity of radiomic data (such as texture and shape), allowing the model to utilize these features without requiring extensive feature selection [30].

In this research, the analysis is based on the top 20 most informative radiomic features selected for their diagnostic accuracy in differentiating malignant from benign endometrial tumors (see **Fig.2** and **Fig. 5**). These features, extracted from preoperative CT scans, encompass texture, shape, and intensity characteristics that

significantly improve classification accuracy. Multiscale texture features, including first-order statistics and GLCM features derived from "log-sigma" (LoG) scales, capture density variations and subtle intensity differences across different scales [31]. These features are closely associated with the heterogeneous tissue structures characteristic of malignant tumors. First-order features, such as the "Range", offer insights into spatial distribution and intensity variance within lesions. Furthermore, wavelet-decomposed features like the "wavelet-LL_firstorder_Range" and "wavelet-LH_glrIm_RunLengthNonUniformity" enhance the model's ability to detect irregular tissue patterns, further improving its precision in distinguishing benign from malignant structures [26]. This combination of features supports a non-invasive, nuanced assessment of EC, enabling a more personalized approach to diagnostic and therapeutic planning.

Current intelligent imaging diagnostic models face significant challenges in clinical practice, primarily due to poor interpretability and the "black box" nature of these models. Therefore, enhancing model interpretability is a prerequisite for clinical adoption. In this study, we utilized two visualization techniques—SHAP feature analysis and radiomics feature maps—to assist the model in EC prediction. This approach can also serve as a reference for other studies.

Despite the encouraging results, this study has several limitations. The sample size is limited, restricts the model's generalizability as it may not fully capture the diversity of EC presentations. Additionally, the data were sourced from only two hospital, potentially introducing bias and limiting the model's applicability across different

imaging settings, equipment, and healthcare environments. To enhance robustness, future research could benefit from larger, more diverse datasets, improving the model's generalizability in varied clinical settings.

Conclusion

In this study, we developed multiple machine learning models based on radiomic features from CT imaging to differentiate between malignant and benign lesions in EC. The results demonstrated that CT-based radiomics analysis achieved high diagnostic accuracy, making it a promising intelligent auxiliary tool for the diagnosis of EC. Notably, the random forest model exhibited the best diagnostic performance. This suggests that combining radiomics from CT imaging with advanced machine learning algorithms can significantly improve early diagnostic accuracy for EC, thereby aiding clinicians in making more precise decisions and potentially improving patient outcomes.

Abbreviations

EC: Endometrial Cancer

LND: Lymphadenectomy

CT: Computed Tomography

MRI: Magnetic Resonance Imaging

PACS: Picture Archiving and Communication System

ROI: Region of Interest

RFE: Recursive Feature Elimination

GLCM: Gray Level Co-occurrence Matrix

GLRLM: Gray Level Run Length Matrix

GLSZM: Gray Level Size Zone Matrix

GLDM: Gray Level Dependence Matrix

NGTDM: Neighboring Gray-Tone Difference Matrix

AUC: Area Under the Curve

ROC: Receiver Operating Characteristic

DCA: Decision Curve Analysis

MMR-D: Mismatch Repair Deficiency

TMB-H: Tumor Mutation Burden-High

RF: Random Forest

LR: Logistic Regression

KNeighbor: K-Nearest Neighbors

SVC: Support Vector Classifier

Compliance with Ethical Standards

Our work was approved by the institutional ethics committee of Qingdao Hiser Hospital.

Conflict of Interest

The authors declare that they have no conflict of interest.

Acknowledgments

This work was financially supported by the Shandong Province Traditional Chinese Medicine Science and Technology Project (M-2022012) and Chengdu Health Commission Medical Health Project (No.2022667).

References

- [1] Miller K.D., Nogueira L., Devasia T., Mariotto A.B., Yabroff K.R., Jemal A., Kramer J., Siegel R.L. Cancer treatment and survivorship statistics, 2022. *CA Cancer J. Clin.* 2022; 72:409–436.
- [2] Makker V., MacKay H., Ray-Coquard I., Levine D.A., Westin S.N., Aoki D., Oaknin A. Endometrial cancer. *Nat. Rev. Dis. Primers.* 2021; 7:88.
- [3] Siegel R.L., Miller K.D., Wagle N.S., Jemal A. Cancer statistics, 2023. *CA Cancer J. Clin.* 2023; 73:17–48.
- [4] Sbarra, M., Lupinelli, M., Brook, O. R., Venkatesan, A. M., & Nougaret, S. Imaging of endometrial cancer. *Radiologic Clinics of North America.* 2023; 61(4):609-625.
- [5] Burbos, N., Musonda, P., Giarenis, I., Shiner, A. M., & Morris, E. P. Predicting the risk of endometrial cancer in postmenopausal women presenting with vaginal bleeding: the Norwich DEFAB risk assessment tool. *British Journal of Cancer.* 2012; 106(9):1611-1616.
- [6] Lin MY, Dobrotwir A, McNally O, Abu-Rustum NR, Narayan K. Role of imaging in the routine management of endometrial cancer. *Int J Gynaecol Obstet.* 2018;143:109–17.
- [7] Barretina-Ginesta, M. P., Quindós, M., Alarcón, J. D., Esteban, C., Gaba, L., Gómez, C., Pérez Fidalgo, J. A., Romero, I., Santaballa, A., & Rubio-Pérez, M. J. (2022). SEOM–GEICO clinical guidelines on endometrial cancer. *Clinical*

Guides in Oncology. 2021; 24:625–634.

- [8] Hodneland, E., Andersen, E., Wagner-Larsen, K.S. et al. Impact of MRI radiomic feature normalization for prognostic modelling in uterine endometrial and cervical cancers. *Sci Rep.* 2024; 14:16826.
- [9] Azeroual, S., Ben-Bouazza, Fe., Naqi, A. et al. Predicting disease recurrence in breast cancer patients using machine learning models with clinical and radiomic characteristics: a retrospective study. *J Egypt Natl Canc Inst.* 2024; 36, 20.
- [10] Ji J, Ju S and Cai W. Editorial: Radiomics-based theranostics in cancer precision medicine. *Front. Oncol.* 2023; 13:1250079.
- [11] Barretina-Ginesta, M. P., Quindós, M., Alarcón, J. D., Esteban, C., Gaba, L., Gómez, C., Pérez Fidalgo, J. A., Romero, I., Santaballa, A., & Rubio-Pérez, M. J. SEOM-GEICO clinical guidelines on endometrial cancer. *Clinical Guides in Oncology.* 2022; 24:625-634.
- [12] Sbarra, M., Lupinelli, M., Brook, O. R., Venkatesan, A. M., & Nougaret, S. Imaging of Endometrial Cancer. *Radiologic Clinics of North America.* 2023; 61(4):609-625.
- [13] NCCN Guidelines Updates for Endometrial Cancer Management. *Journal of the National Comprehensive Cancer Network.* 2024; 22(Suppl):49-50.
- [14] Williams, L. E., Zheng, Y., Voss, E. A., & Gillies, R. J. Radiomic features from CT images as predictive biomarkers for endometrial cancer aggressiveness. *Academic Radiology.* 2022; 29(2):273-282.
- [15] Veeraraghavan, H., Lee, S., Karlan, B. Y., & Tavassoli, F. A. Advanced deep learning techniques in MRI-based diagnosis of endometrial cancer. *Journal of Magnetic Resonance Imaging.* 2021; 53(1):188-197.

-
- [16] Smith, A. B., Jones, J. C., Roberts, J., Lee, D. K., & Challis, B. G. Comparative analysis of machine learning algorithms in the MRI-based diagnosis of endometrial cancer. *Radiology*. 2020; 295(3):215-224.
- [17] Aerts, H. J. W. L. et al. Decoding tumour phenotype by noninvasive imaging using a quantitative radiomics approach. *Nature Communications*. 2014; 5:4006.
- [18] Esteva, A., Kuprel, B., Novoa, R. A., Ko, J., Swetter, S. M., Blau, H. M., & Thrun, S. Dermatologist-level classification of skin cancer with deep neural networks. *Nature*. 2017; 542(7639):115-118.
- [19] Litjens, G., Sánchez, C. I., Timofeeva, N., Hermsen, M., Nagtegaal, I., Kovacs, I., Hulsbergen-Van de Kaa, C., Bult, P., Van Ginneken, B., & Van Der Laak, J. Deep learning as a tool for increased accuracy and efficiency of histopathological diagnosis. *Scientific Reports*. 2016; 6:26286.
- [20] Urban, G., Tripathi, P., Alkayali, T., Mittal, M., Jalali, F., Karnes, W., & Baldi, P. Deep learning localizes and identifies polyps in real time with 96% accuracy in screening colonoscopy. *Gastroenterology*. 2018; 155(4):1069-1078.e8.
- [21] Veeraraghavan, H., Friedman, C.F., DeLair, D.F. et al. Machine learning-based prediction of microsatellite instability and high tumor mutation burden from contrast-enhanced computed tomography in endometrial cancers. *Sci Rep*. 2020; 10, 17769.
- [22] Coda CA, Santoro M, Zybin V, Di Stanislao M, Paolani G, Modolon C, Di Costanzo S, Genovesi L, Tesei M, De Leo A, Ravegnini G, De Biase D, Morganti AG, Lovato L, De Iaco P, Strigari L, Perrone AM. A Radiomic-Based Machine Learning Model Predicts Endometrial Cancer Recurrence Using Preoperative CT Radiomic Features: A Pilot Study. *Cancers (Basel)*. 2023; 15(18):4534.
- [23] Morice P, Leary A, Creutzberg C, et al. Endometrial cancer. *The Lancet*. 2016; 387(10023): 1094-1108.

-
- [24] Wang L, Wen D, Yin Y, et al. Musculoskeletal ultrasound image - based radiomics for the diagnosis of Achilles tendinopathy in skiers. *Journal of Ultrasound in Medicine*. 2023, 42(2): 363-371.
- [25] Xie J, Yang Y, Jiang Z, et al. MRI radiomics-based decision support tool for a personalized classification of cervical disc degeneration: a two-center study. *Frontiers in Physiology*. 2024; 14:1281506.
- [26] Jiang Z, Yin J, Han P, Chen N, Kang Q, Qiu Y, Li Y, Lao Q, Sun M, Yang D, Huang S, Qiu J, Li K. Wavelet transformation can enhance computed tomography texture features: a multicenter radiomics study for grade assessment of COVID-19 pulmonary lesions. *Quant Imaging Med Surg*. 2022;12(10):4758-4770.
- [27] Hollmann N, Müller S, Purucker L, et al. Accurate predictions on small data with a tabular foundation model. *Nature*. 2025; 637(8045): 319-326.
- [28] Ye, R., Jiang, Z., Shao, R., Yan, Q., Zhou, L., Zhang, T., & Sun, Y. Development and validation of tongue imaging-based radiomics tool for the diagnosis of insomnia degree: a two-center study. *Medical Data Mining*. 2024;7(1):4.
- [29] Carrington A M, Manuel D G, Fieguth P W, et al. Deep ROC analysis and AUC as balanced average accuracy, for improved classifier selection, audit and explanation. *IEEE Transactions on Pattern Analysis and Machine Intelligence*. 2022; 45(1): 329-341.
- [30] Jiang Z, Wang B, Han X, Zhao P, Gao M, Zhang Y, Wei P, Lan C, Liu Y, Li D. Multimodality MRI-based radiomics approach to predict the posttreatment response of lung cancer brain metastases to gamma knife radiosurgery. *Eur Radiol*. 2022; 32(4):2266-2276.

-
- [31] Dong Y, Jiang Z, Li C, Dong S, Zhang S, Lv Y, Sun F, Liu S. Development and validation of novel radiomics-based nomograms for the prediction of *EGFR* mutations and Ki-67 proliferation index in non-small cell lung cancer. *Quant Imaging Med Surg.* 2022;12(5):2658-2671.

Tables
Table 1 Patient demographic characteristics

Characteristics	Groups	Full Cohort (n=84)	Training Set (n=59)	Testing Set (n=24)	<i>P</i>
Age (years)	Mean \pm	57.46	56.66	59.42	0.218
	SD	8.99	8.86	9.20	
Gender	Male	0	0	0	1.000
	Female	84	59	24	
Diagnosis Type	Benign	37	26	11	0.886
	Malignant	46	33	13	

Table 2 Top 20 radiomic features comparison of experimental and control groups

Num	Radiomic Features	Experimental Group Mean \pm SD	Control Group Mean \pm SD	<i>P</i>
F1	LoG-5-0-mm-firstorder_90Percentile	0.8973 \pm 2.7674	-0.9706 \pm 0.7182	<0.001
F2	wavelet-LH_firstorder_Maximum	33.2488 \pm 33.5727	14.9921 \pm 4.8543	0.003
F3	squareroot_glcmln	0.9718 \pm 0.0198	0.9596 \pm 0.0121	0.005
F4	LoG-1-0-mm-glcmln_MaximumProbability	0.3875 \pm 0.0577	0.4283 \pm 0.0250	0.001
F5	squareroot_gldm_DependenceNonUniformity	16142.3282 \pm 11937.4632	8633.8018 \pm 6180.8670	0.003
F6	wavelet-HL_firstorder_Maximum	28.4411 \pm 25.4365	13.6784 \pm 9.4997	0.003
F7	LoG-3-0-mm-glcmln_MaximumProbability	0.5927 \pm 0.1446	0.6951 \pm 0.0667	0.001
F8	log-sigma-3-0-mm-3D_glrmln_GrayLevelNonUniformity	4232.4170 \pm 3772.8624	2097.2949 \pm 1207.3108	0.003
F9	wavelet-LH_glrmln_RunLengthNonUniformity	26007.2400 \pm 16713.7003	14698.5115 \pm 10658.1750	0.002
F10	LoG-1-0-mm-firstorder_Maximum	28.3740 \pm 28.7366	11.7850 \pm 4.5883	0.002
F11	log-sigma-3-0-mm-3D_glcmln_JointEnergy	0.4245 \pm 0.1408	0.5147 \pm 0.0848	0.003
F12	original_glcmln_MaximumProbability	19854.2579 \pm 14212.2986	12160.5326 \pm 4979.3845	0.005
F13	wavelet-LH_firstorder_Range	71.2081 \pm 65.8776	33.7422 \pm 10.9061	0.002
F14	wavelet-HL_glrmln_RunLengthNonUniformity	19522.2754 \pm 14082.0266	10815.4521 \pm 7310.8897	0.003
F15	original_firstorder_Range	112.8110 \pm 92.6035	56.7198 \pm 24.6335	0.001
F16	wavelet-LL_firstorder_Range	211.0077 \pm 173.9878	104.9770 \pm 50.7249	0.001
F17	log-sigma-1-0-mm-3D_glcmln_JointEnergy	0.2717 \pm 0.0507	0.3003 \pm 0.0148	0.003
F18	log-sigma-1-0-mm-3D_glrmln_ShortRunEmphasis	0.3876 \pm 0.1447	0.3087 \pm 0.0430	0.004
F19	wavelet-LH_ngtdm_Complexity	96.3095 \pm 142.3560	18.9783 \pm 12.6605	0.003
F20	log-sigma-3-0-mm-3D_firstorder Uniformity	0.4881 \pm 0.1366	0.5699 \pm 0.0797	0.005

Table 3 Performance comparison of various machine learning models for classification

Model	Dataset	AUC	Sensitivity (%)	Specificity (%)	Accuracy (%)	Precision (%)
Logistic Regression	Training	0.95	88.57	87.50	88.14	91.18
	Testing	0.95	100.00	92.31	95.83	91.67
K-Neighbors	Training	0.94	82.86	91.67	86.44	93.55
	Testing	0.94	81.82	92.31	87.5	90.00
SVC	Training	0.97	94.29	91.67	93.22	94.29
	Testing	0.95	100.00	92.31	95.83	91.67
XGBoost	Training	1.00	100.00	100.00	100.00	100.00
	Testing	0.88	72.73	92.31	83.33	88.89
TabPFNv2	Training	1.00	100.00	100.00	100.00	100.00
	Testing	0.96	81.82	92.31	87.50	90.00
Random Forest	Training	1.00	100.00	95.83	98.31	97.22
	Testing	0.96	100.00	92.31	95.83	91.67

Figures

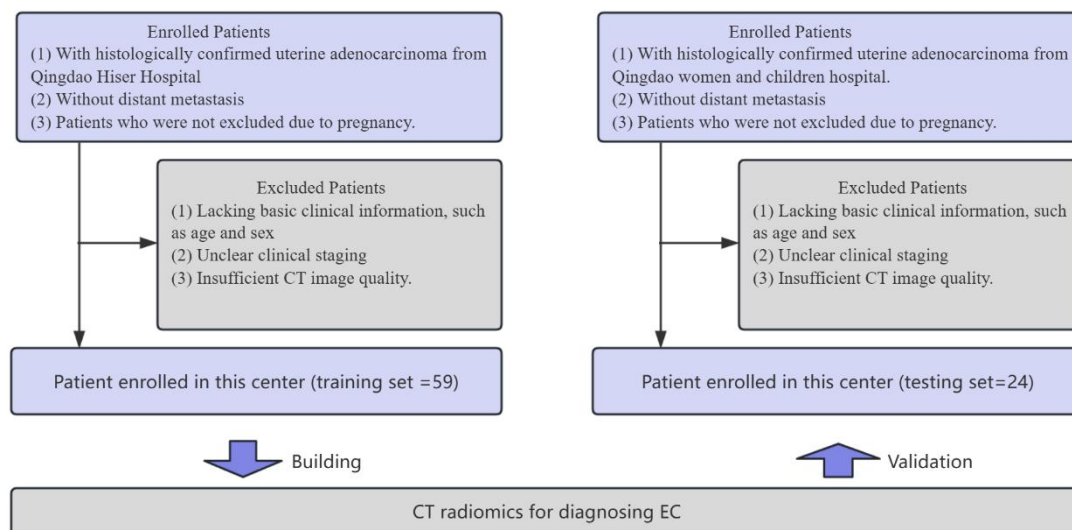


Fig.1 Patient inclusion and exclusion criteria flowchart.

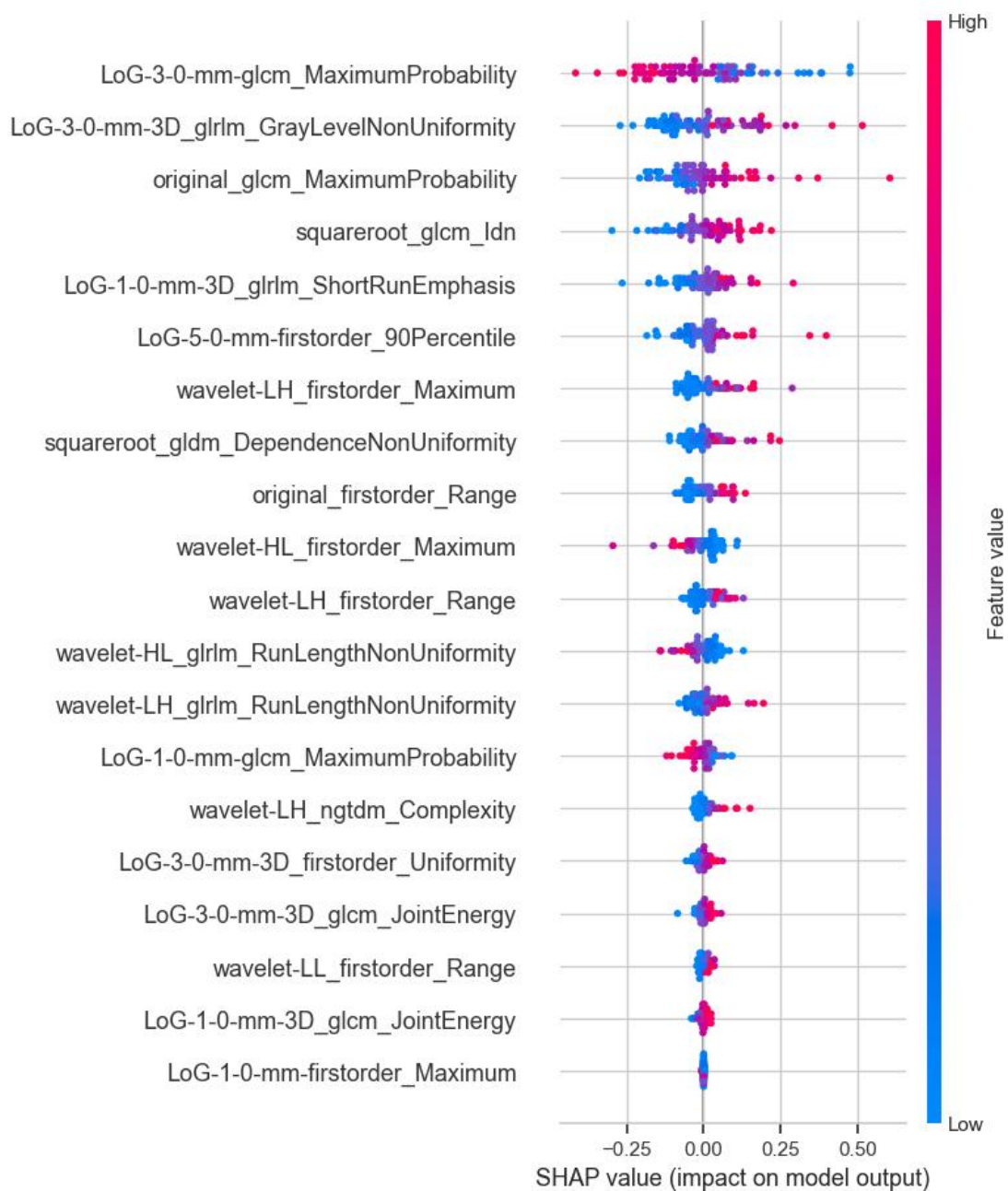


Fig. 2 SHAP analysis of the Top 20 radiomic features.

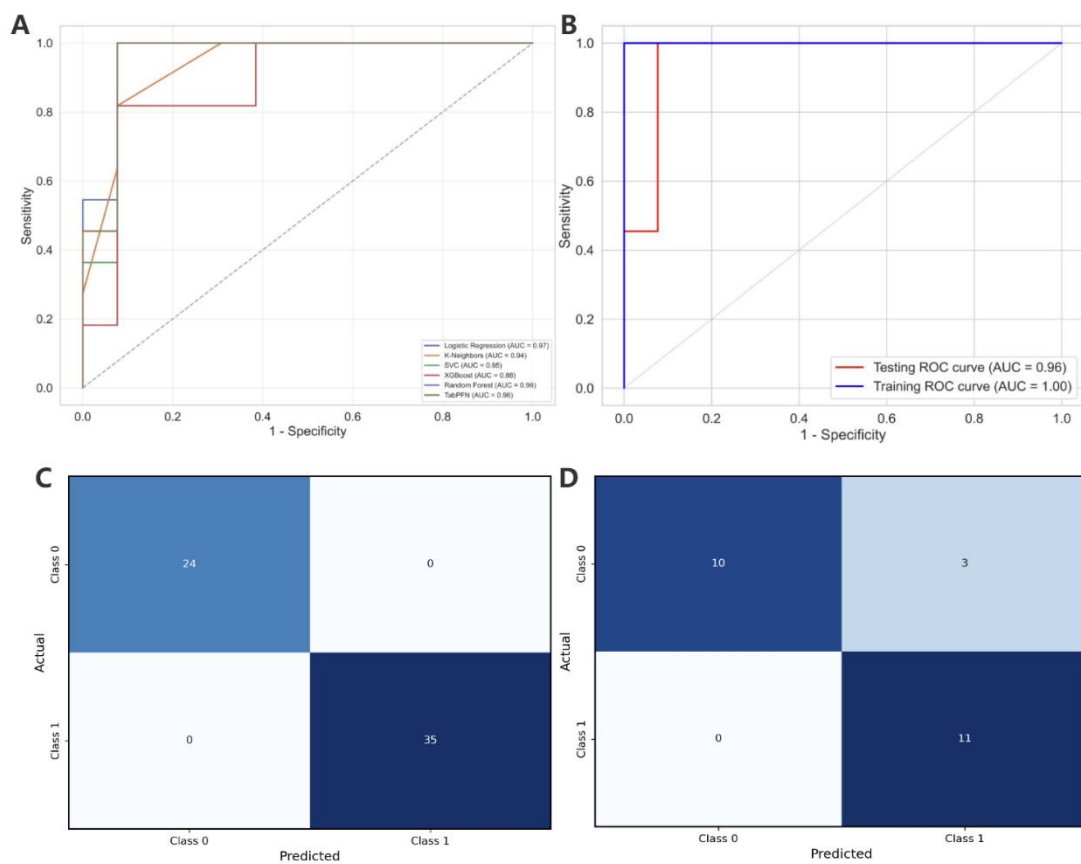


Fig. 3 ROC curves and confusion matrices of machine learning models. (A) ROC curves for comparing various models. (B) ROC curves for the best-performing Random Forest model on training and testing sets. (C) Training set confusion matrix for the best model. (D) Testing set confusion matrix for the best model.

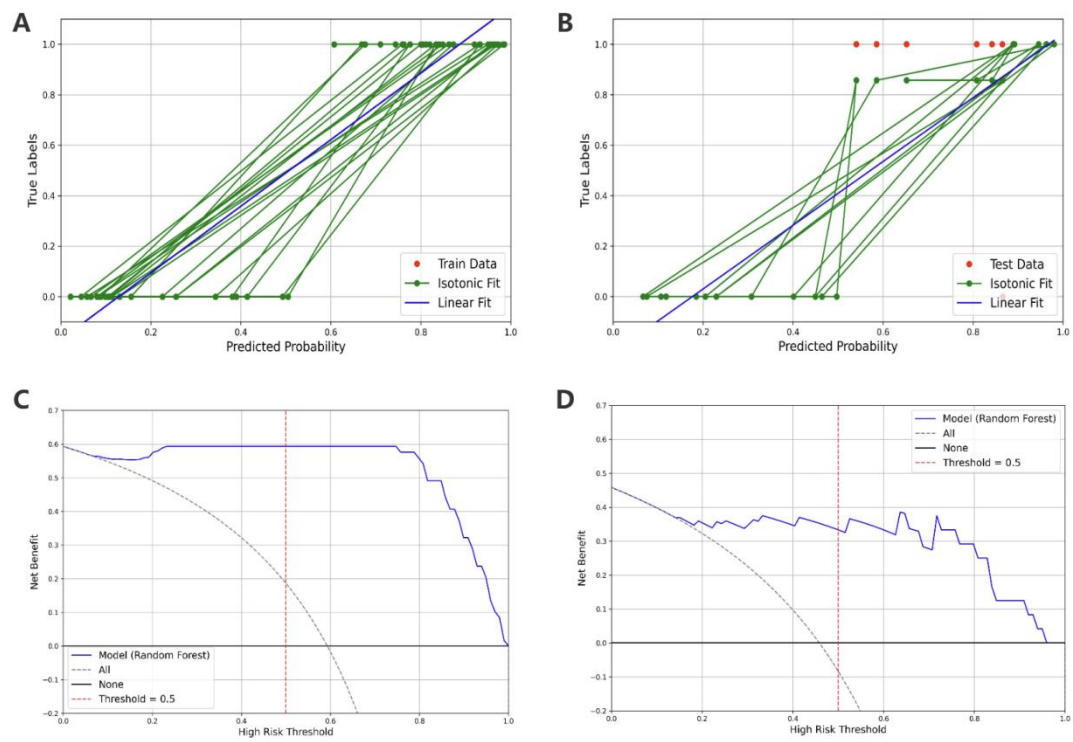


Fig. 4 Calibration curves and decision curves for the final model. Calibration curves in (A) training set and (B) testing set. Decision curves in the (C) training set and (D) testing set.

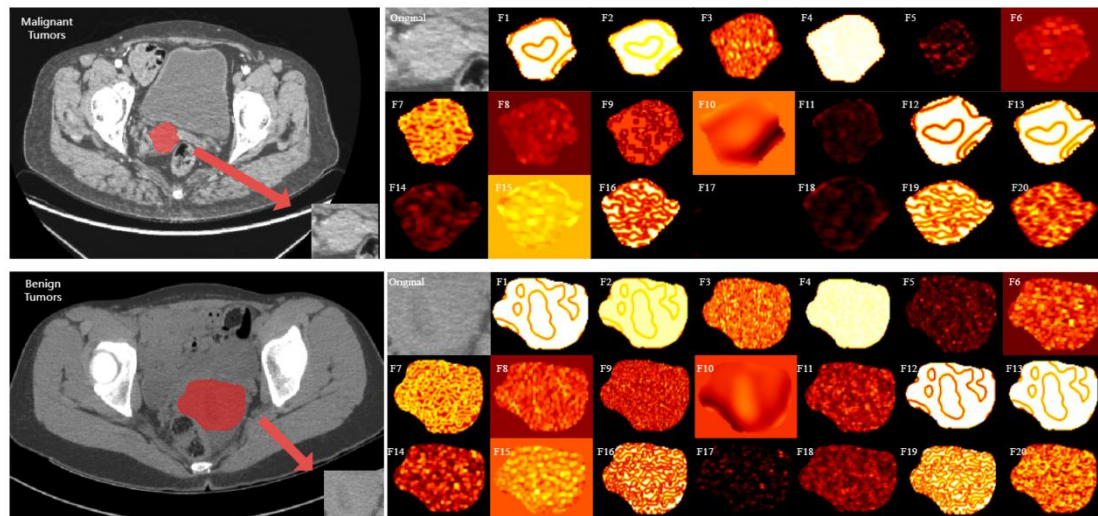


Fig. 5 Two representative cases demonstrating the precise prediction of EC malignancy and benignity using our model, with 20 radiomics feature maps.